

# Radio frequency tomography for passive indoor multi-target tracking

Santosh Nannuru, Yunpeng Li, Yan Zeng, Mark Coates, and Bo Yang

**Abstract**—Radio Frequency (RF) tomography is the method of tracking targets using received signal-strength (RSS) measurements for RF transmissions between multiple sensor nodes. When the targets are near the line-of-sight path between two nodes, they are more likely to cause substantial attenuation or amplification of the RF signal. In this paper, we develop a measurement model for multi-target tracking using (RF) tomography in indoor environments and apply it successfully for tracking up to three targets. We compare several multi-target tracking algorithms and examine performance in the two scenarios when the number of targets is (i) known and constant; and (ii) unknown and time-varying. We demonstrate successful tracking for experimental data collected from sensor networks deployed in three different indoor environments posing different tracking challenges. For the case of a fixed number of targets, the best algorithm achieves a root mean squared error tracking accuracy of approximately 0.3m for a single target, 0.7m for two targets and 0.8m for three targets. Tracking using our proposed model is more accurate than tracking using previously proposed observation models; more importantly the model does not require the same degree of training.

**Index Terms**—Radio frequency tomography, multi-target tracking, indoor setup, device-free passive localization, particle filters.

## 1 INTRODUCTION

WE address the task of tracking multiple mobile targets in an indoor environment. We are interested in a “device-free” setting where the targets have no direct communication with the tracking system. Applications of such a tracking system can be found in military surveillance, search-and-rescue operations, through the wall imaging, and healthcare environments [1], [2].

Radio-frequency (RF) tomography is the process of monitoring an area to detect mobile targets based on the additional attenuation and fluctuations they cause in wireless transmissions [3]. Wireless networks of radio-frequency (RF) sensors can be easily deployed and are relatively inexpensive. Compared to the other available alternatives such as infrared and video, RF measurements have the advantage that they can penetrate walls and other non-metallic obstacles.

In this paper we propose a multi-target measurement model for the RF tomography problem in an indoor setting. The indoor environment is significantly more challenging than the outdoor environment because of the multiple obstructions and the multipath effects caused by reflections from walls, ceilings, furniture, etc. These differences cause the outdoor

multi-target measurement model developed in [4] to perform poorly when used in an indoor setting.

We first demonstrate that single-target tracking using the proposed model outperforms tracking using the skew-Laplace model developed in [5]. The performance difference is more considerable for multiple targets; the skew Laplace model is much more sensitive to parameter choices.

For the proposed model, we successfully demonstrate tracking of up to three targets when the number of targets present in the network is known. In many practical scenarios we expect the targets to be continuously entering and leaving the scene of interest, thus tracking a time varying number of targets is of practical importance. We demonstrate successful tracking of up to two targets when their number is unknown and varies over time. We compare the performance of four candidate multi-target tracking algorithms: the bootstrap particle filter [6], the multiple particle filter [7], the Markov Chain Monte Carlo (MCMC) filter [8], [9], and the Additive Likelihood Moment (ALM) filter [9]<sup>1</sup>. When the target number is known we compare all the above algorithms and when the target number varies with time we compare the bootstrap filter and the MCMC filter.

The remainder of the paper is organized as follows. In Section 2 we briefly review related work. We formalize the indoor multi-target tracking problem in Section 3. Section 4 describes and discusses the proposed indoor multi-target measurement model and reviews previously-developed models. Section 5

- S. Nannuru and M. Coates are with the Department of Electrical and Computer Engineering, McGill University, Montreal, Quebec. E-mail: santosh.nannuru@mail.mcgill.ca, mark.coates@mcgill.ca.
- Y. Li, Y. Zeng and B. Yang are with the School of Information and Communication Engineering, Beijing University of Posts and Telecommunications, Beijing, China. E-mail: liyp@bupt.edu.cn, zengyan\_js@bupt.edu.cn, boyang@bupt.edu.cn.

1. An error in the original publication [9] has been corrected and is available in the errata [10]; the correction was also provided in [11].

provides a brief overview of the tracking algorithms we compare. Section 6 describes the experiments we conducted and examines the tracking performance. In Section 7 we conclude and identify future research directions.

## 2 LITERATURE REVIEW

Device-free Passive (DfP) localization of targets using wireless sensor networks has recently received significant attention. A good overview of the challenges faced in realizing a DfP system and the different techniques for target localization can be found in the review paper [2]. RF tomography systems have several desirable aspects. They are relatively cheap and simple to deploy. The measurements do not have the same privacy concerns as video, and they can penetrate walls and non-metallic objects.

Most previous RF tomography tracking techniques have focused on single target tracking. In [3], [12] Wilson and Patwari proposed an inverse imaging algorithm which first obtains an attenuation map and then applies a Kalman filter to track the peak in the map. Li et al. introduced a new measurement model based on experimental data and use it in a sequential Monte Carlo algorithm for tracking [13]. This method incorporated online Expectation-Maximization so that model parameters could be learned during the tracking task. This approach was extended in [14] to simultaneously estimate the locations of the sensor nodes.

Thouin et al. address the multi-target tracking problem for super-positional sensors in [9]. They propose a measurement model for RF sensors that assumes that targets cause additive attenuation effects. The model was experimentally validated in [4] for multiple targets using data collected from outdoor sensor network deployments. Accurate tracking of up to four targets in a relatively uncluttered outdoor environment is also demonstrated using the additive model.

Zhang et al. developed an indoor multi-target tracking system for ceiling-mounted RF sensor nodes based on the interference caused by moving objects [15], [16], [17]. These systems achieve good tracking performance but require calibration and are restricted to the ceiling deployment of sensors. This is not practical in several important scenarios (search-and-rescue, military surveillance).

More recently in [5], Wilson and Patwari developed a skew-Laplace signal strength model for indoor target tracking. Received signal-strength (RSS) measurements are modeled using skew-Laplace distributions whose parameters are experimentally obtained through training measurements. The parameters change depending on whether the target is close to the line-of-sight between the sensors. Successful tracking of two targets (fixed and known number) was reported in [5], but the case of an unknown and time-varying number of targets was not addressed. The

model parameters need to be trained using a target with known position; Wilson and Patwari suggest that parameters learned in one environment can be applied successfully in another. Our experiments indicated that this strategy led to numerous lost tracks, particularly in the multi-target setting.

## 3 PROBLEM STATEMENT

RF Tomography relies on the RSS measurements of wireless packets exchanged between the sensors in the network. These measurements are affected by the distance between the sensors and the disturbance caused by static and moving objects. When multiple links monitor a region, the relative RSS measurements among the different links can be used to localize moving objects.

We consider a network of  $R$  nodes with  $M = \frac{R(R-1)}{2}$  bidirectional links. Each bidirectional link records an RSS measurement. At time step  $k$ , the RSS measurement on link  $i$  is denoted by  $\gamma_i(k)$  and it is the average of the RSS values recorded on the forward and reverse links. The individual link measurements are stacked into a vector  $\gamma_k$ . We subtract from  $\gamma_k$  a vector  $\tilde{\gamma}$ , where  $\tilde{\gamma}_i$  is the average RSS on link  $i$  when no target is present. In order to estimate the average RSS  $\tilde{\gamma}_i$ , we assume there is a time period when RSS measurements can be captured from the empty network when no targets are present. If such a period does not exist, these values can also be estimated using techniques based on background subtraction [18]. The change in RSS  $z_k = \tilde{\gamma} - \gamma_k$  is the measurement available to the tracker at time step  $k$ .

We now state the RF tomography tracking problem. Let there be  $N_k$  targets present in the sensed region with the state of the  $n^{\text{th}}$  target given by  $x_{k,n}$ . The combined state is given by the set  $X_k = \{x_{k,1}, x_{k,2}, \dots, x_{k,N_k}\}$ . We assume that the state of each target evolves independently and is specified by a Markovian dynamic model  $f_{k|k-1}(x_{k,n}|x_{k-1,n})$ . The goal of RF Tomography is to estimate the posterior distribution at every time step  $k$  of all the targets present in the network given the measurements up to time  $k$ ,  $p(X_k|z^{(1:k)})$ , where  $z^{(1:k)}$  represents all the observations up to time  $k$ , i.e.,  $z^{(1:k)} = \{z_1, z_2, \dots, z_k\}$ . We can derive point estimates of the state from the estimates of the posterior.

## 4 MEASUREMENT MODELS

We now discuss different measurement models that can be used in an indoor setting. We first review the exponential model that has been used successfully to track targets [4] outdoors but fails in an indoor environment. We propose a modification to suit indoor settings and describe its extension to the multiple target case. We also review the skew-Laplacian model from [5] and suggest a minor modification which leads to better tracking results in our experiments.

## 4.1 Exponential model

Li et al. proposed a single target measurement model for RF tomography based on experimental data from relatively uncluttered outdoor regions [13]. The mean of the attenuation on link  $j$  caused by a target at position  $x_k$  is modeled as

$$g_j(x_k) = \phi \exp\left(-\frac{\lambda_j(x_k)}{\sigma_\lambda}\right) \quad (1)$$

where  $\phi$  and  $\sigma_\lambda$  are attenuation parameters based on physical properties of the targets and sensors. The value  $\lambda_j(x_k)$  is defined as

$$\lambda_j(x_k) = d_1(x_k) + d_2(x_k) - d_{12} \quad (2)$$

where  $d_1(x_k)$  and  $d_2(x_k)$  are the distances between the target and the two sensors and  $d_{12}$  is the distance between the sensors.  $\lambda_j(x_k)$  captures a notion of the distance between the target and the line-of-sight link between transmitter and receiver. The observed noisy attenuation values are modeled as  $z_k = g(x_k) + w_k$ , where  $g = [g_1, g_2, \dots, g_M]$ , and  $w_k$  is noise, distributed according to  $\mathcal{N}(0, \Sigma = \sigma_w^2 I_{M \times M})$ , where  $I_{M \times M}$  is the identity matrix and  $\sigma_w^2$  is the noise variance.

Thouin et al. proposed a multi-target extension of this model in [9]; the model was validated using experimental data for outdoor environments in [4]. The mean attenuation caused by the presence of multiple targets is modeled as equal to the sum of the mean attenuations due to each of the targets. Denote by  $g_j(x_{k,n})$  the attenuation on link  $j$  due to the  $n^{\text{th}}$  target located at  $x_{k,n}$ . Then the mean of the total attenuation on link  $j$  due to all of the targets combined is modeled as:

$$g_j(X_k) = \sum_{n=1}^{N_k} g_j(x_{k,n}) \quad (3)$$

where  $N_k$  is the total number of targets within the field of observation at time  $k$ . The observed noisy attenuation values are given by

$$z_k = g(X_k) + w_k \quad (4)$$

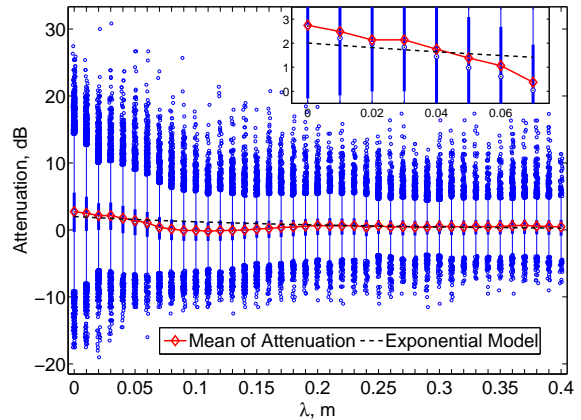
## 4.2 Magnitude model

In an outdoor environment, a link usually experiences attenuation when a target is nearby. However, due to the multi-path effects in the indoor environment, a link can experience either attenuation or amplification when people move nearby. The model outlined above does not capture amplification. To address this, we choose to model the attenuation amplitude  $y_k = |z_k|$  using the model:

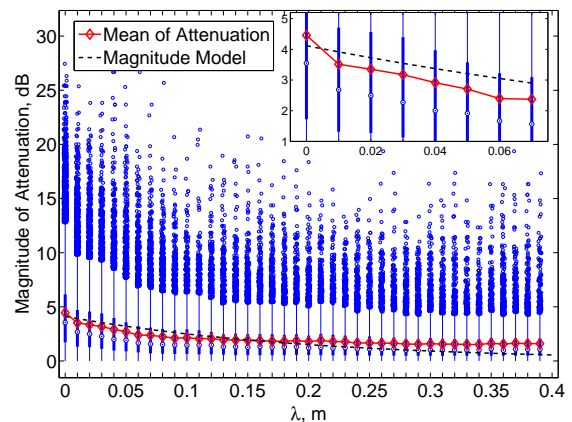
$$Pr(y_k|x_k) \propto \mathcal{N}(g(x_k), \sigma_w^2 I_{M \times M}) \quad \text{for } y_k > 0 \quad (5)$$

Here  $g(x_k)$  has the same form as in (1), but the parameter values are generally significantly different for indoor and outdoor environments.

Figures 1(a) & 1(b) display box-and-whisker plots of the attenuation and its magnitude, for single target



(a) Indoor data with exponential model



(b) Indoor data with the magnitude model

Figure 1. Box plots of the attenuation (top) and its magnitude (bottom) from Experiment 1 (see Section 6). Overlaid are the exponential and magnitude models.

data recorded in Experiment 1 (see Section 6). The data are binned according to the  $\lambda$  values; for each bin, the box ranges from the 25th to 75th percentile, the circle within the box indicates the median value, and the circles beyond the whiskers indicate outliers. Overlaid are the exponential and magnitude models, with parameters fitted using linear regression.

Both models achieve a relatively good fit to the means when  $\lambda$  is small, which is the important region. However, the magnitude model has a higher slope (see inset figures) and can thus more easily discern when the target is close to a link. For human targets, we have observed that the best-fit model parameters are similar for multiple indoor environments (with  $\phi$  ranging from 3 – 7, and  $\sigma_\lambda$  ranging from 0.2 – 0.4). Tracking performance is relatively robust to the parameter choice.

Figure 1(b) illustrates that the attenuation measurements are very noisy, with numerous outliers and heavy tails. The Gaussian noise model does not capture the tails particularly accurately (the skew-

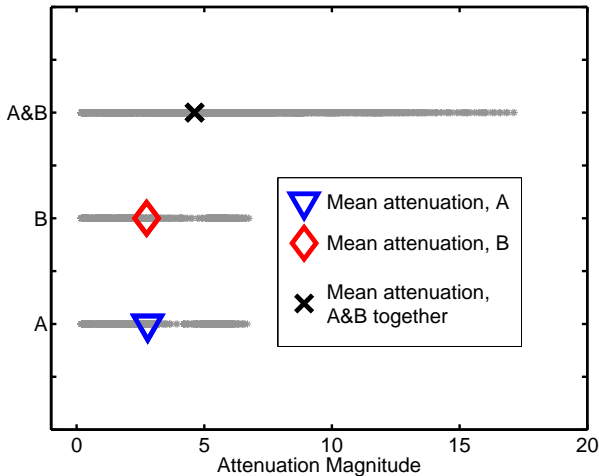


Figure 2. Magnitude of RSS attenuation when one or two targets are present along the line-of-sight of a single link; experiments were conducted for a link in Setup 2 (see Section 6). Scattered points depict attenuation values averaged over short intervals and the markers indicate the mean values.

Laplacian is a more accurate model in this regard), but it is sufficient for tracking purposes and is more computationally tractable.

Similar to (3), we propose a multi-target extension to the magnitude model. The magnitude of the attenuation  $y_k$  is modeled as:

$$Pr(y_k|x_k) \propto \mathcal{N}(g(X_k), \sigma_w^2 I_{M \times M}) \quad \text{for } y_k > 0 \quad (6)$$

where  $g(X_k)$  and  $w_k$  are the same as above. We thus model the observed attenuation magnitude as sum of predicted attenuations caused by the individual targets and corrupted by Gaussian noise.

Experimental support for this additive model is provided in Figure 2. Data was collected from a single indoor link of 7 meters (a representative link from Setup 2 in Section 6), comparing the cases where one target or two targets obstruct the link along its line-of-sight. Target A stood at different locations along the link and we recorded approximately 15,000 measurements of the resultant RSS attenuation. The procedure was repeated for target B at slightly different locations. We then made measurements with both A and B present at different combinations of the locations. The mean attenuation values are 2.78 and 2.74 for the individual targets, and 4.62 for the two targets. The distribution of attenuations for a combination of targets has a significantly heavier tail; a more sophisticated model could strive to capture this effect in addition to the increased mean.

### 4.3 Skew Laplacian model

In [5], Wilson et al. proposed the use of the skew-Laplace distribution to model RSS attenuation. The

$\lambda$	Parameter		
	a	b	$\psi$
$0 < \lambda \leq 0.2$	$0.78\lambda + 0.41$	$1.40\lambda + 0.24$	$-1.47\lambda + 0.35$
$\lambda > 0.2$	1.29	1.08	-0.01

Table 1

Parameter values for fitted skew-Laplace distributions.

skew-Laplace likelihood is defined as:

$$\begin{aligned} p(z_k|x_k) &= p(z_k|x_k; a, b, \psi) \\ &= \begin{cases} \frac{ab}{a+b} e^{-a(\psi-z_k)}, & \text{if } z_k \leq \psi \\ \frac{ab}{a+b} e^{-b(z_k-\psi)}, & \text{otherwise} \end{cases} \quad (7) \end{aligned}$$

Here  $a$  and  $b$  represent the one-sided decay rates of the distribution for values less than or greater than the mode  $\psi$ . The parameters  $a$ ,  $b$  and  $\psi$  are modeled as linearly dependent on the “fade level” [5] for each link. The fade level quantifies the amount of fading when no targets are present and is estimated using measurements performed during a training period. Different linear fits are obtained depending on whether or not the target is on the line-of-sight path; this classification depends on a distance threshold.

We conducted experiments in three different indoor locations (see Section 6) and collected more than three million data points. We observed that the RSS attenuation distributions vary as the value of  $\lambda$  changes. Modifying the model proposed in [5], we model the parameters  $a$ ,  $b$ , and  $\psi$  as linear functions of  $\lambda$ . For  $\lambda < 0.2$ , we divide the attenuation measurements into bins of width 0.01 in terms of  $\lambda$ ; conduct a grid-search to identify the best-fit skew-Laplace parameters for each bin; and perform linear regression on these best-fit parameters to obtain linear models. Figure 3 and Table 1 show the fits we obtain. For  $\lambda > 0.2$ , the target location has little impact on the RSS measurement and we model the parameters as constant.

The upward trends of parameters  $a$  and  $b$  indicate that the distribution tends to become more peaky as  $\lambda$  increases (there are fewer large-magnitude attenuations/amplifications). For the parameter  $\psi$  (not shown), the trend is less noticeable, but exhibits a downward trend, reflecting our observation that amplifications become rarer as  $\lambda$  increases. In later measurement based simulations we will compare the original skew-Laplace model [5] and the modified model proposed in this section.

## 5 TARGET TRACKING ALGORITHMS

We now discuss several particle-based multi-target tracking algorithms. Algorithms such as the extended or unscented Kalman filter do not perform well because the likelihood function is highly non-linear.

### 5.1 Tracking with target number ( $N_k$ ) known

Knowing the number of targets allows for a simplified implementation of the tracking algorithms. We com-

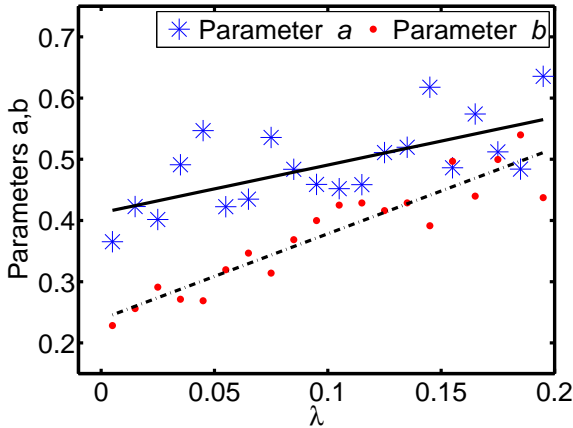


Figure 3. Linear fits to the skew-Laplace parameters  $a$  and  $b$  obtained using training data from all three single-target experiments described in Section 6. The  $*$  and  $\cdot$  markers show the best fit values for each  $\lambda$  bin.

pare four different filters. The first is based on the principle of sequential importance resampling (SIR) and is commonly known as the bootstrap filter [6]. Since many practitioners are familiar with it we do not discuss it in detail. In brief, at every time step, the SIR filter maintains a weighted set of particles to approximate the marginal posterior distribution. Resampling (drawing a new set of unweighted particles from the weighted set) is performed periodically to maintain diversity of the particle set.

The particle filter can perform poorly when the state has high dimension, which occurs with multiple targets. To address this, Bugallo et al. proposed the multiple particle filter (MPF) [7], which uses one low-dimensional particle filter for each target (see Figure 4). The filter runs for  $T$  steps, processing one measurement vector at each time step. For each of the  $N$  targets the MPF maintains a separate particle filter using  $N_p$  particles. We implement each of these as an SIR filter. The weight update step for the individual filters cannot be performed independently of the other target states because computing the measurement likelihood requires the combined state information. The MPF uses an estimate for the other target states,  $\hat{X}_{k,\underline{n}} = \{\hat{x}_{k,1} \dots \hat{x}_{k,n-1}, \hat{x}_{k,n+1} \dots \hat{x}_{k,N}\}$ , where  $\hat{x}_{k,j}$  is a weighted average of the current particles  $\{x_{k,j}^{(i)}\}$  using the weights from the previous time step  $\{w_{k-1,j}^{(i)}\}$ .

The third algorithm we assess is the Markov Chain Monte Carlo (MCMC) filter of [8] (see Figure 5). Samples (particles) are drawn at each time step by sequentially traversing a Markov chain which has the desired marginal posterior as its stationary distribution. The Joint Draw step is implemented using the Metropolis-Hastings algorithm. The Refinement step uses Gibbs sampling to sequentially update each

```

1: Initialize  $N$  particle filters  $\{w_{0,n}^{(i)}, x_{0,n}^{(i)}\}_{i=1}^{N_p}$ 
2: for  $k = 1$  to  $T$  do
3:   for  $n = 1$  to  $N$  do
4:     for  $i = 1$  to  $N_p$  do
5:       proposal step:
6:        $x_{k,n}^{(i)} \sim p(x_{k,n} | x_{k-1,n}^{(i)})$ 
7:       estimation step:
8:        $\hat{x}_{k,n} \approx \sum_{i=1}^{N_p} w_{k-1,n}^{(i)} x_{k,n}^{(i)}$ 
9:     end for
10:  end for
11:  for  $n = 1$  to  $N$  do
12:    for  $i = 1$  to  $N_p$  do
13:      weight update:
14:       $w_{k,n}^{(i)} \propto w_{k-1,n}^{(i)} p(z_k | x_{k,n}^{(i)}, \hat{X}_{k,\underline{n}})$ 
15:      resample step:
16:       $\{w_{k,n}^{(i)}, x_{k,n}^{(i)}\}_{i=1}^{N_p} \rightarrow \{\frac{1}{N_p}, x_{k,n}^{(i)}\}_{i=1}^{N_p}$ 
17:    end for
18:  end for
19: end for

```

Figure 4. Multiple Particle Filter (MPF) [7].

target state. The proposal densities  $q_1$  and  $q_2$  are:

$$q_1(X_k, X_{k-1} | X_k^{m-1}, X_{k-1}^{m-1}) \propto \prod_{i=1}^{N \times N_p} f_{k|k-1}(X_k | X_{k-1}^{(i)}) \delta(X_{k-1}^{(i)}) \quad (8)$$

$$q_2(x_{k,n} | X_{k,\underline{n}}^m, X_{k-1}^m) = f_{k|k-1}(x_{k,n} | x_{k-1,n}^m) \quad (9)$$

where  $X_{k,\underline{n}} = \{x_{k,1} \dots x_{k,n-1}, x_{k,n+1} \dots x_{k,N}\}$ . To sample from  $q_1$  we uniformly randomly choose a particle at time  $k-1$  from the set  $\{X_{k-1}^{(i)}\}$  and propagate it following the target Markovian dynamics  $f_{k|k-1}$ . At every time step, the MCMC chain is initialized with a particle from the previous time step that has the highest likelihood for the current observation.  $\rho_1$  and  $\rho_2$  are the acceptance probabilities for joint draw and refinement steps of the algorithm. A burn-in of  $N_{burn}$  samples and a thinning factor of  $N_{thin}$  reduce the correlation between the consecutive samples.

The final filter we assess is the Additive Likelihood Moment (ALM) filter [9] (see Figure 6). The algorithms discussed earlier either try to sample from the joint target posterior density (SIR and MCMC) or from the individual target marginal posterior densities (MPF), but the ALM filter samples from the first moment of the joint target posterior density, also called the Probability Hypothesis Density (PHD) [19]. This is a function over the single target state space. It is high in regions where targets are present and its integral over the target state space is equal to the expected number of targets. Thus sampling from the PHD populates particles in region where there is high probability of targets being present. The advantage of the ALM filter is that we do not have to sample from the high

```

1: Initialize particles  $\{X_0^{(i)}\}_{i=1}^{N \times N_p}$ 
2: for  $k = 1$  to  $T$  do
3:   Initialize MCMC chain  $(X_k^{(0)}, X_{k-1}^{(0)})$ 
4:   for  $m = 1$  to  $(N_{burn} + N_p \times N \times N_{thin})$  do
5:     Joint Draw
6:      $(X_k^*, X_{k-1}^*) \sim q_1(X_k, X_{k-1} | X_k^{m-1}, X_{k-1}^{m-1})$ 
7:      $(X_k^m, X_{k-1}^m) = (X_k^*, X_{k-1}^*)$  with prob.  $\rho_1$ 
8:     else  $(X_k^m, X_{k-1}^m) = (X_k^{m-1}, X_{k-1}^{m-1})$ 
9:     Refinement
10:    for  $n = 1$  to  $N$  do
11:      draw  $x_{k,n}^* \sim q_2(x_{k,n} | X_{k,n}^m, X_{k-1}^m)$ 
12:      refine  $x_{k,n}^m = x_{k,n}^*$  with prob.  $\rho_2$ 
13:    end for
14:    Selection
15:    for  $i = 1$  to  $N_p \times N$  do
16:       $X_k^{(i)} = X_k^{N_{burn} + i \times N_{thin}}$ 
17:    end for
18:  end for
19: end for

```

Figure 5. MCMC Filter [8]

dimensional space of multiple targets. The ALM filter provides a particle representation of the PHD at each time step; to form estimates of target states we use  $k$ -means clustering to group the particles into clusters, each of which corresponds to a target.

```

1: Initialize particles  $\{w_0^{(i)}, x_0^{(i)}\}_{i=1}^{N \times N_p}$ 
2: for  $k = 1$  to  $T$  do
3:   for  $i = 1$  to  $N \times N_p$  do
4:     proposal:  $x_k^{(i)} \sim f_{k|k-1}(x_k | x_{k-1}^{(i)})$ 
5:      $w_{k|k-1}^{(i)} = w_{k-1}^{(i)}$ 
6:   end for
7:    $\hat{\mu}_k = \sum_j w_{k|k-1}^{(j)} g(x_k^{(j)})$ 
8:    $\hat{\Sigma}_k = \sum_j w_{k|k-1}^{(j)} g(x_k^{(j)}) g^T(x_k^{(j)})$ 
9:   for  $i = 1$  to  $N \times N_p$  do
10:    weight update:
11:    
$$F_k(x_k^{(i)}) = \frac{\mathcal{N}_{z_k}(\hat{\mu}_k, \hat{\Sigma}_k + \Sigma)}{\mathcal{N}_{z_k}(g(x_k^{(i)}) + \hat{\mu}_k, \hat{\Sigma}_k + \Sigma)}$$

12:    
$$w_k^{(i)} = \frac{w_{k|k-1}^{(i)}}{F_k(x_k^{(i)})}$$

13:   end for
14:   resample step:
15:    $\{w_k^{(i)}, x_k^{(i)}\}_{i=1}^{N \times N_p} \rightarrow \left\{ \frac{1}{N \times N_p}, x_k^{(i)} \right\}_{i=1}^{N \times N_p}$ 
16:   clustering step:
17:    $\{\hat{x}_{k,n}\}_{n=1}^N = \text{cluster}(\{x_k^{(i)}\}_{i=1}^{N \times N_p}, N)$ 
18: end for

```

Figure 6. ALM Filter [9]

## 5.2 Tracking with target number ( $N_k$ ) unknown

We now discuss an extension of the SIR and MCMC filters which allows them to address the case where the number of targets is unknown and varies with

time. Following [20], we extend each target state to include an indicator variable  $e_{k,n}$  which indicates the presence or absence of the target. Thus the target state is now given by  $\{x_{k,n}, e_{k,n}\}$ . In our analysis we assume that the indicator variable evolves independently of the target location and velocity and does so independently for each of the targets. This approach requires us to specify the maximum number of targets  $N_{max}$  that can be present at any given time. The SIR and MCMC algorithms presented above are easily modified; there is just an additional propagation step for the indicator variable. Since the number of targets is unknown, we need to estimate the number of targets as well as the target locations. We employ a simple heuristic: at any time step we declare a target to be present if more than half of the corresponding target particles have their indicator variable set to 1.

## 6 EXPERIMENTS AND RESULTS

### 6.1 Target dynamics and tracking parameters

A jump-state Markov model is a standard model for describing the dynamics of a maneuvering object [21], [22]. The model assumes that the target operates at each time step in one of multiple modes of operation (represented as a discrete state variable). The discrete state jumps/switches are independent of the target positions and are governed by a Markov chain.

We adopt the following jump-state Markov model in our experiments. The initial distribution is modeled as  $p(u_0, \theta_0, x_0)$ . The update equations are:

$$u_k \sim p(u_k | u_{k-1}), \quad (10)$$

$$\theta_k = \theta_{k-1} + c(u_k) + s_k, \quad (11)$$

$$x_k = x_{k-1} + m[\cos \theta_k, \sin \theta_k] + v_k. \quad (12)$$

Here  $u_k \in \{0, 1, 2\}$  represents ‘‘no turn’’ ( $c(0) = 0$ ), ‘‘left-turn’’ ( $c(1) = 0.1$  rad), and ‘‘right-turn’’ ( $c(2) = -0.1$  rad), respectively.  $p(u_k | u_{k-1})$  is the transition probability matrix,  $\theta_k$  indicates the current motion angle and  $s_k \sim \mathcal{N}(0, \sigma_s^2)$  and  $v_k \sim \mathcal{N}(0, \sigma_v^2 I_{2 \times 2})$  are the innovation noise terms.  $x_k$  is the position vector and speed of motion is specified by  $m$ .

We set  $m = 0.1$ <sup>2</sup> in our experiments since it approximates walking speed. We model  $p(u_k | u_{k-1})$  as:

$$\begin{pmatrix} 0.75 & 0.65 & 0.65 \\ 0.125 & 0.3 & 0.05 \\ 0.125 & 0.05 & 0.3 \end{pmatrix}$$

The matrix is chosen to approximate typical human motion characteristics. Higher values in the first row indicate a greater tendency to walk straight than to make turns. Angle innovation noise variance  $\sigma_s^2$  is set to 0.001 to model smooth target motion. The tracking performance is robust to small changes in  $\sigma_s^2$ ,  $m$  and the matrix entries. The parameter  $\sigma_v$  is set to 0.1,

2. The effect of changing the velocity parameter  $m$  can be found in the technical report [23].

although we examine the impact of changing it to 0.2 for the single-target case.

Observation model parameters were selected based on training phases performed at the three experimental sites. The test data sets do not include any data from the training phases. For the MCMC filter, we use  $N_{burn} = 1000$  and  $N_{thin} = 3$ , which are standard values from the literature, observed to be sufficient in many cases to substantially reduce correlation between samples.

## 6.2 Experimental setup

We performed multiple experiments at three different experiment sites and repeated each experiment multiple (8-10) times. The first site is in the Trottier Building at McGill University (Figure 7(b)). An area of  $8m \times 8m$  was monitored by 24 sensor nodes (Figure 7(a)). It is referred to as Setup1 henceforth. A concrete pillar lies within the network. The second experiment site (Setup2) is the Computer Networks Lab of McGill University (Figure 7(d)). An area of  $9m \times 9m$  is monitored by 24 sensor nodes (Figure 7(c)). Numerous desks and chairs are present within the network and there are walls just outside. The third experiment site (Setup3) is in the Beijing University of Posts and Telecommunications (BUPT), China. Data was collected in a completely through-wall environment (Figure 7(f)) using 28 nodes covering a  $5.2m \times 6.7m$  region (Figure 7(e)).

We performed multiple single and multi-target experiments. The single target experiments at Setup1, Setup2 and Setup3 are respectively referred to as "Exp. 1", "Exp. 2" and "Exp. 3". The two-target experiments at Setup1 and Setup2 are called "Exp. 4" and "Exp. 5" respectively. The three-target experiment at Setup1 is called "Exp. 6". The time-varying number of targets experiment at Setup2 is called "Exp. 7". The setup description and experiments are summarised in Table 2.

Setup	Experiment		Description
Setup1	Exp. 1	single target	24 sensors in $8m \times 8m$ , concrete pillar obstruction
	Exp. 4	two target	
	Exp. 6	three target	
Setup2	Exp. 2	single target	24 sensors in $9m \times 9m$ , desks and chairs obstruction
	Exp. 5	two target	
	Exp. 7	two target, time varying	
Setup3	Exp. 3	single target	28 sensors in $5.2m \times 6.7m$ , through-wall environment

Table 2

Description of the different indoor experimental setups and the nature of the experiments used to collect data.

The transceivers of the sensor nodes are system-on-chip (SoC) TI CC2530 devices; each node has a monopole antenna and uses the 2.4 GHz IEEE 802.15.4 standard for communication. A simple token ring

protocol is used to control transmission. A single measurement interval corresponds to the period required for all nodes to transmit (200ms). During each time interval of 6.7 ms, one node broadcasts a data packet. All of the other nodes receive this packet and measure the RSS. The token is then passed to the next node.

Some links exhibit large variance in their RSS measurements even when the network is vacant. Those links have severe impacts on the tracking results, as the variation of the RSS is not caused by the targets. Thus we exclude the RSS measurements of any links whose variance is higher than 1 for the vacant network as a pre-processing step.

## 6.3 Tracking performance

To compare and evaluate the algorithms, we need metrics to measure the deviation of the estimated tracks from the ground truth tracks. When the number of targets is fixed we use the optimal mass transfer (OMAT) metric [24]. The  $p$ -th order OMAT metric is:

$$d_p(X, Y) = \left( \frac{1}{n} \min_{\pi \in \Pi} \sum_{i=1}^n d(x_i, y_{\pi(i)})^p \right)^{1/p} \quad (13)$$

where  $\Pi$  is the set of possible permutations of  $\{1, 2, \dots, n\}$  and  $d(x, y)$  is the Euclidean distance between  $x$  and  $y$ .  $X = \{x_1, \dots, x_n\}$  and  $Y = \{y_1, \dots, y_n\}$  are arbitrary sets and  $p$  is a fixed parameter. We use the value  $p = 2$ . The OMAT metric uses the permutation of the target location estimates which minimizes the mean squared error from the true locations.

The OMAT metric is unsuitable for a time-varying number of targets because it does not penalize errors in the estimation of the number of targets. The optimal subpattern assignment (OSPA) metric [24] adds an additional term ( $c$ ) which penalizes the cardinality error. When there are  $n$  targets and we estimate  $m$  targets then for  $m \leq n$  the OSPA metric is

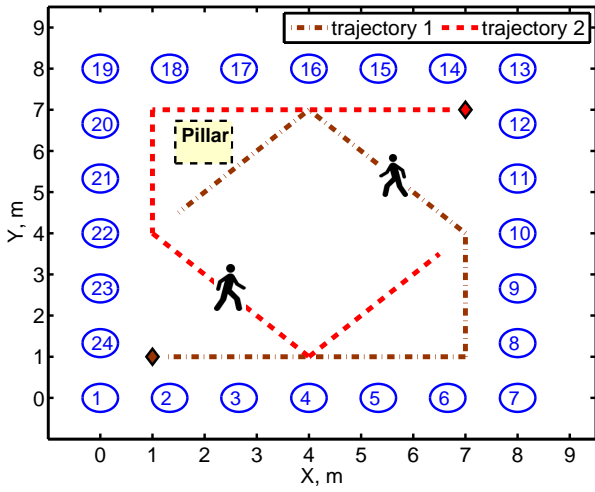
$$d_p^{(c)}(X, Y) = \left( \frac{1}{n} \min_{\pi \in \Pi} \sum_{i=1}^m d^{(c)}(x_i, y_{\pi(i)})^p + c^p(n - m) \right)^{1/p} \quad (14)$$

where  $d^{(c)}(x, y) = \min\{d(x, y), c\}$ ,  $X = \{x_1, \dots, x_m\}$  and  $Y = \{y_1, \dots, y_n\}$ . When  $m > n$ , we calculate  $d_p^{(c)}(Y, X)$ . The OSPA metric finds the best permutation of the larger set which minimizes its distance from the smaller set and assigns a fixed penalty for each cardinality error.

The reported tracking errors are calculated by averaging over the multiple repetitions of the experiments and for each experiment running the tracking algorithm with 10 different random initializations.

### 6.3.1 Single target tracking

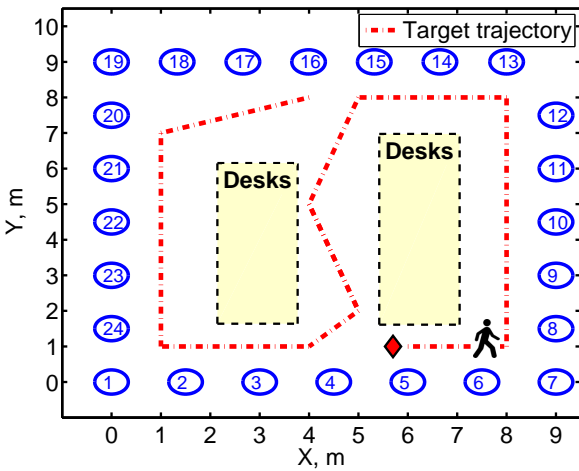
Table 3 summarizes the tracking performance for the different single target experiments using the algorithms of SIR, MCMC and ALM. For all filters, we



(a) Setup1 layout.



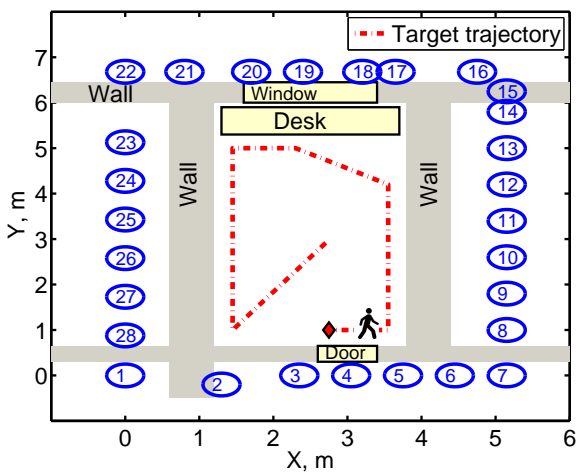
(b) Photograph of Setup1.



(c) Setup2 layout.



(d) Photograph of Setup2.

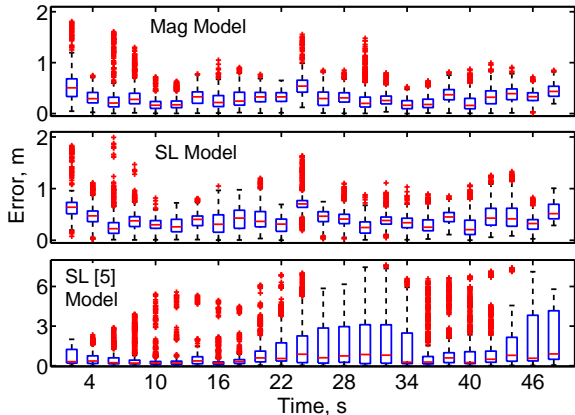


(e) Setup3 layout.

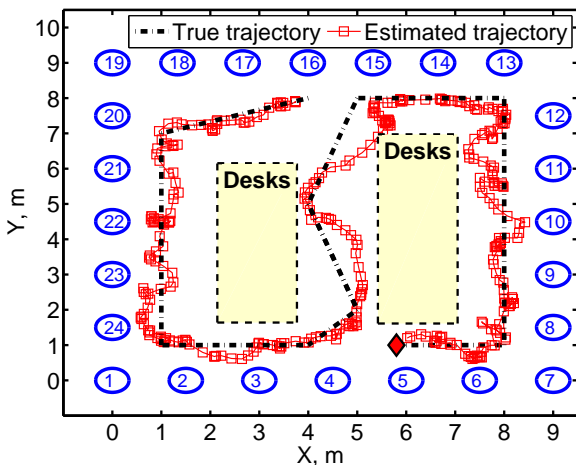


(f) Photograph of Setup3.

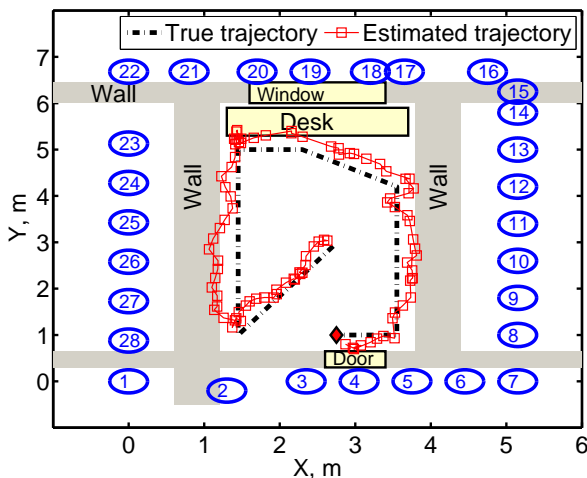
Figure 7. Layouts and photos of the three experiments: (a), (b) Setup1 (uncluttered indoor environment); (c), (d) Setup2 (cluttered indoor environment); (e), (f) Setup3 (through-wall measurements).



(a) Exp. 1 error for different measurement models



(b) Exp. 2.



(c) Exp. 3.

Figure 8. (a) Box-and-whisker plot of the OMAT error over time for the Exp.1 data using the MCMC algorithm. (b), (c) Sample single target trajectories using the magnitude model in different indoor environments. The small diamond indicates the start of trajectory.

set  $N_p = 500$  (larger values were observed to give minimal improvement and smaller values lead to larger tracking error). The MPF is identical to the SIR algorithm in the single target case. Tracking is performed using the measurement models discussed in Section 4: the magnitude model (Mag), modified skew-Laplace model (SL) and original skew-Laplace model (SL [5]). We detail the best-fit skew-Laplace parameters for the three experimental sites in [25]. For the magnitude model, we use  $\sigma_w = 2$ ,  $\phi = 4$  and  $\sigma_\lambda = 0.2$ . Since the particle implementation of the ALM filter in [9] is obtained assuming the measurement noise to be Gaussian, we do not perform its skew-Laplacian analysis.

Two different values of the innovation noise standard deviation,  $\sigma_v = 0.1$  and  $\sigma_v = 0.2$ , are considered to analyze the robustness of the measurement models. A higher value of  $\sigma_v$  implies less confidence in the motion model; it also facilitates recovery from tracking errors. Table 3 suggests the original skew-Laplace model performance is sensitive to the choice of  $\sigma_v$ . In most cases the magnitude model has a lower error than the modified skew-Laplace model, which in turn generally performs better than the original skew-Laplace model. The magnitude model is relatively insensitive to the choice of  $\sigma_v$  for both the SIR and MCMC algorithms. The SIR and MCMC have similar performance and both perform better than the ALM filter. Figures 8(b) and 8(c) plot sample target trajectories obtained using the SIR filter and the magnitude model for the three different experiments.

Exp.	SIR			MCMC			ALM
	Mag	SL	SL [5]	$\sigma_v = 0.1$			
Exp. 1	<b>0.31</b>	0.35	2.73	<b>0.31</b>	0.40	1.06	0.45
Exp. 2	<b>0.41</b>	1.01	3.10	<b>0.37</b>	0.46	1.50	0.50
Exp. 3	<b>0.36</b>	0.56	1.55	<b>0.30</b>	0.37	0.37	0.46
$\sigma_v = 0.2$							
Exp. 1	<b>0.35</b>	0.38	0.54	<b>0.32</b>	0.40	0.34	0.53
Exp. 2	<b>0.43</b>	0.47	0.59	<b>0.41</b>	0.45	0.46	0.56
Exp. 3	<b>0.34</b>	0.45	0.41	0.30	0.36	<b>0.29</b>	0.54

Table 3

Single target: Average error (in meter) using different tracking algorithms and different measurement models for Exp. 1, Exp. 2, and Exp. 3.  $\sigma_v = 0.1, 0.2$ . Data partitioned into training and testing data set.

Figure 8(a) shows the OMAT error over time using a box-and-whisker diagram for the MCMC algorithm ( $\sigma_v = 0.1$ ). Boxes range from the 25<sup>th</sup> to 75<sup>th</sup> percentile, the line within the box indicates the median value, and the pluses indicate outliers. Using the original skew-Laplace model, there are multiple lost tracks; with the modified model, performance is comparable to the magnitude model. The computational time requirements of the tracking algorithms also play an important role in their practical applicability. Table 4 summarizes the average normalized processing times

of each of the algorithms with different measurement model combinations. The normalized processing time is the ratio of time required to process the data<sup>3</sup> to the duration of the experiment. A normalized time less than 1 indicates a real-time performance of the algorithm. The SIR, MPF and ALM algorithms are computationally fast and can perform real time tracking when a single target is present.

Exp.	SIR			MCMC			ALM
	Mag	SL	SL [5]	Mag	SL	SL [5]	Mag
Exp. 1	<b>0.19</b>	0.45	0.50	6.79	22.79	26.06	0.38
Exp. 2	<b>0.11</b>	0.24	0.37	13.19	22.70	25.11	0.63
Exp. 3	<b>0.12</b>	0.34	0.41	7.79	13.58	15.80	0.46

Table 4

Single target: Average normalized processing time using different tracking algorithms and different measurement models for Exp. 1, Exp. 2, and Exp. 3.

### 6.3.2 Multiple target tracking with known and fixed number of targets

We now consider tracking experiments in which there are multiple (two or more) targets and the number of targets is fixed and known. Two-target experiments were performed at Setup1 and Setup2 and a three-target experiment was conducted at Setup1. We examined the performance of the skew-Laplace measurement model for multiple targets but it frequently leads to lost tracks and has significantly higher average error for all algorithms. Hence, in this section, we only report results for the multi-target magnitude measurement model discussed in Section 4.2. We use the model parameters  $\sigma_w = 2$ ,  $\phi = 3$  and  $\sigma_\lambda = 0.4$ .

Tables 5 and 6 report the average OMAT errors for the two-target experiments, Exp. 4 and Exp. 5. To examine the effect of prior information on the overall tracking performance, we consider two different initial particle distributions. For the ‘‘Informed Prior’’, we initialize the particles at the first time step according to a Gaussian distribution with variance 1, centered at the true target locations. In the ‘‘Uniform Prior’’, we initialize the particles uniformly at random within the observation region.

The MPF performs best when the ‘‘Informed Prior’’ is used. For all the methods except ALM the average error reduces as the number of particles is increased. There is minimal gain in accuracy for any algorithm if the number of particles per target is increased beyond  $N_p = 750$ . The error fluctuations for the ALM filter with respect to the number of particles are due primarily to errors during the clustering stage.

When the particles are initialized using the non-informative ‘‘Uniform Prior’’, the SIR and MPF al-

Exp. 4	$N_p$	SIR	MPF	MCMC	ALM
Informed Prior	100	1.46	1.00	<b>0.86</b>	0.93
	250	1.05	<b>0.79</b>	0.83	0.86
	500	0.92	<b>0.67</b>	0.80	0.88
	750	0.80	<b>0.62</b>	0.80	0.88
Uniform Prior	100	1.63	1.78	1.06	<b>0.96</b>
	250	1.27	1.58	1.00	<b>0.89</b>
	500	1.06	1.44	0.97	<b>0.91</b>
	750	1.01	1.36	0.92	<b>0.91</b>

Table 5

Two targets: Average error (in meters) using different algorithms with  $N_p = 100, 250, 500$  &  $750$  for Exp. 4, Setup1.

Exp. 5	$N_p$	SIR	MPF	MCMC	ALM
Informed Prior	100	1.11	0.94	<b>0.72</b>	0.93
	250	1.00	0.82	<b>0.70</b>	0.92
	500	0.83	<b>0.71</b>	<b>0.70</b>	0.89
	750	0.72	<b>0.70</b>	<b>0.69</b>	0.88
Uniform Prior	100	1.15	1.21	<b>0.74</b>	0.92
	250	0.94	1.01	<b>0.72</b>	0.89
	500	0.88	0.92	<b>0.72</b>	0.91
	750	0.80	1.00	<b>0.72</b>	0.89

Table 6

Two targets: Average error (in meters) using different algorithms with  $N_p = 100, 250, 500$  &  $750$  for Exp. 5, Setup2.

gorithm performances worsen significantly for Experiment 4. The MCMC algorithm is more robust with respect to the prior information, and the ALM filter displays little sensitivity to the initialization. The computational requirements of the different algorithms are displayed in Table 7. Results for both cases ‘‘Informed Prior’’ and ‘‘Uniform Prior’’ were observed to be similar and hence we report only for the latter. The SIR, MPF (500 particles or less) and ALM filter (250 particles or less) can execute in real-time. The MCMC algorithm has a major computational overhead and cannot execute in real-time with the current implementation and processor.

Figures 9(a) and 9(b) show sample target trajectories obtained using the MPF algorithm in Exp. 4 and Exp. 5 respectively. Figure 10 displays box-and-whisker OMAT error plots for the Exp. 4 data for the four tracking algorithms. The boxes range from the 25<sup>th</sup> to 75<sup>th</sup> percentiles, the line within the box indicates the median value, and the pluses indicate outliers.

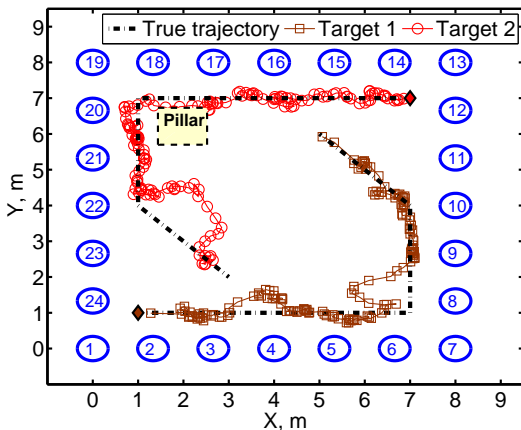
Table 8 reports the average OMAT error for Exp. 6 data when three targets are simultaneously present. When using the ‘‘Informed Prior’’, the MPF algorithm has the lowest tracking error. When the ‘‘Uniform Prior’’ is used, the ALM filter performs noticeably better than the other algorithms. The ALM filter operates in the single-target state space; increasing the number of targets has less impact on its performance. The corresponding computational time requirements for the algorithms are summarized in Table 9. Real-time

3. All the processing has been performed using algorithms implemented in Matlab on Two Xeon 4-core 2.5GHz, 14GB RAM computers.

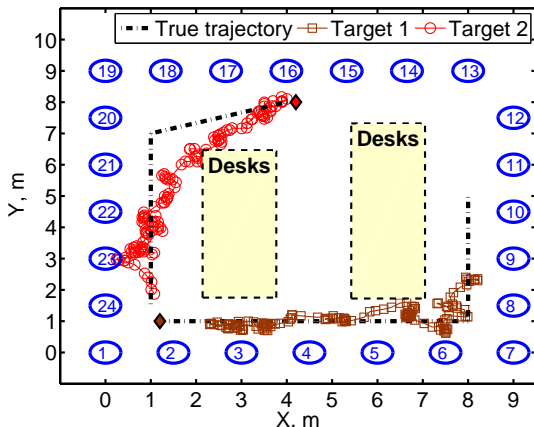
Exp. 4	$N_p$	SIR	MPF	MCMC	ALM
Uniform Prior	100	0.12	0.11	16.42	0.61
	250	0.34	0.30	25.97	0.95
	500	0.75	0.68	41.81	1.57
	750	1.23	1.10	57.41	2.21
Exp. 5					
Uniform Prior	100	0.12	0.11	16.37	0.56
	250	0.34	0.30	25.90	0.88
	500	0.76	0.67	41.78	1.44
	750	1.21	1.10	57.68	2.02

Table 7

Two targets: Average normalized processing time using different algorithms with  $N_p = 100, 250, 500$  & 750 for Exp. 4 and Exp. 5.



(a) Exp. 4, Setup1



(b) Exp. 5, Setup2

Figure 9. Example target tracks estimated by the MPF algorithm when two targets are present.

tracking is possible with the SIR and MPF algorithms using 250 particles or less, but this involves some decrease in accuracy. The ALM filter can execute in real time for 100 particles, but its accuracy is less sensitive to the number of particles.

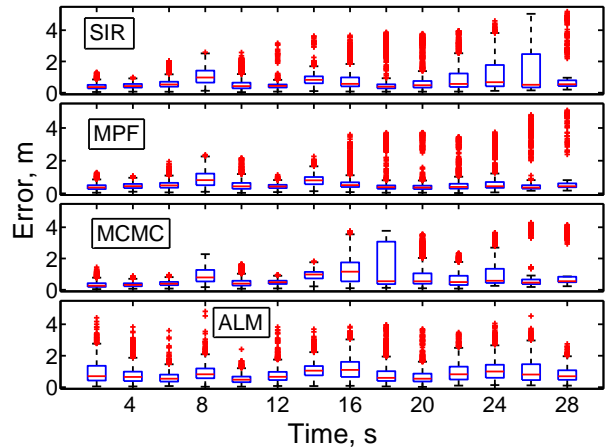


Figure 10. Box-and-whisker plot of OMAT error over time using magnitude model for Exp. 4 data.

Exp. 6	$N_p$	SIR	MPF	MCMC	ALM
Informed Prior	100	1.94	<b>0.75</b>	0.90	0.75
	250	1.34	<b>0.58</b>	0.89	0.76
	500	1.04	<b>0.56</b>	0.84	0.80
	750	0.91	<b>0.54</b>	0.83	0.83
Uniform Prior	100	2.08	1.20	0.98	<b>0.76</b>
	250	1.56	1.07	0.92	<b>0.77</b>
	500	1.09	0.96	0.97	<b>0.83</b>
	750	0.95	1.03	0.91	<b>0.84</b>

Table 8

Three targets: Average OMAT error (meters) for Exp. 6, Setup1.

### 6.3.3 Multiple target tracking with unknown and varying number of targets

We now address the most challenging indoor target tracking task of tracking a time varying number of targets. We use the SIR and MCMC algorithms, adapted to account for varying target number as discussed in Section 5.2, to track the targets. The multi-target magnitude measurement model is used for likelihood computation. We assume the maximum number of targets is  $N_{max} = 4$ . The model parameters are  $\sigma_w = 2$ ,  $\phi = 5$  and  $\sigma_v = 0.1$ .

Table 10 shows the average error values for the Exp. 7 data for different values of the cardinality penalty  $c$ . We set the number of particles per target to  $N_p = 500$  and use the ‘‘Informed Prior’’ particle initialization. When the cardinality penalty is small ( $c = 1$ ), the error is comparable to the two-target error when the number of targets is known, indicating that the tracking performance of the algorithms is not significantly affected by the missing information. Both the algorithms have similar error values for small  $c$  and MCMC error increases slightly with  $c$  indicating the MCMC cardinality estimate is not as robust as the SIR. More sophisticated methods to estimate cardinality rather than the simple heuristic method we currently employ are expected to give better results.

Exp. 6	$N_p$	SIR	MPF	MCMC	ALM
Uniform Prior	100	0.29	0.25	31.49	0.86
	250	0.83	0.69	54.51	1.48
	500	1.94	1.58	93.63	2.59
	750	2.95	2.45	131.4	3.62

Table 9

Three targets: Average normalized processing time for Exp. 6, Setup1.

Exp. 7	OSPA error		
	$c = 1$	$c = 2.5$	$c = 5$
Algorithm			
SIR	0.60	0.91	1.32
MCMC	0.60	0.93	1.38

Table 10

Varying target number: Average OSPA errors for Exp. 7 data.

Figure 11 compares the actual number of targets to the SIR cardinality estimate. Also shown is the corresponding error variation for  $c = 1$  and  $c = 5$ . The algorithm makes numerous cardinality estimation errors, particularly in the time-period 25-30s, when one of the targets is in the region between the desks (Figure 7(c)) and hence is more difficult to detect.

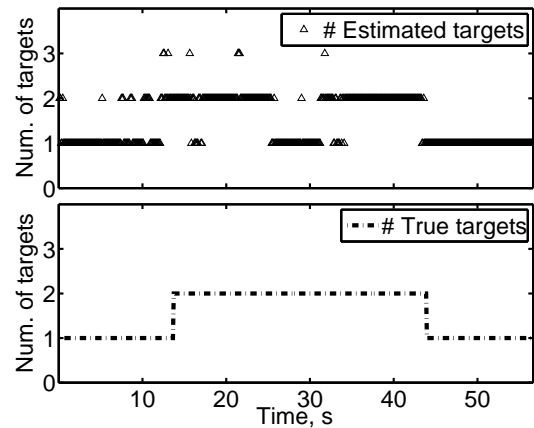
## 7 CONCLUSION

We have presented measurement models and particle-based algorithms for RF-tomographic multi-target tracking in indoor environments. We introduced a modification to the skew-Laplace measurement model of [5] and proposed a new magnitude measurement model. We demonstrated through experiments at three different sites, representing a variety of measurement challenges, that the algorithms can successfully track up to three targets. The algorithms can track a time-varying number of targets, but struggle to estimate the number of targets. The good performance of the ALM filter for the three-target case motivates future exploration of a recently-proposed generalization [11] that explicitly tracks the cardinality.

The system and algorithms can perform well when sensors are deployed inside a room with furniture, or densely deployed outside a small, uncluttered room with thick concrete walls. Through-wall tracking using fewer sensors deployed outside a cluttered, large room remains as an important challenge for these systems and algorithms.

The experiments reported in this work do not address several of the key challenges in multi-target tracking. Further experiments are necessary to explore whether the algorithms can perform well when the targets come together in groups, then separate.

The truncated Gaussian model adopted for the likelihood function does not capture the heavy tails we observe in the distribution of the attenuation measurements. This does not substantially compromise



(a) Target number estimate using SIR

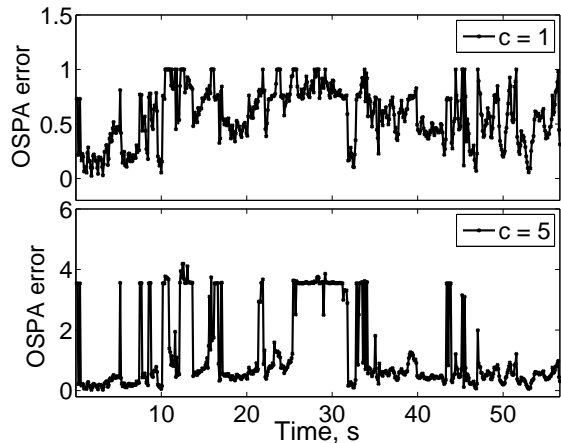
(b) OSPA error with  $c = 1$  and  $c = 5$ 

Figure 11. (a) Example of the true number of targets and the SIR cardinality estimate (Exp. 7, Setup2). (b) Average OSPA error for  $c = 1$  and  $c = 5$ .

performance in the reported experiments because the sensors are relatively densely deployed, but the development of more accurate likelihood models should be explored in future work.

## ACKNOWLEDGMENT

The authors would like to thank Divya Alok Sharma, Rizwan Butt and Arslan Shahid for their help in conducting the experiments at McGill University.

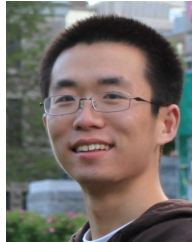
## REFERENCES

- [1] M. Moussa and M. Youssef, "Smart devices for smart environments: device-free passive detection in real environments," in *Proc. Int. Conf. Perv. Comp. Comm.*, Galveston, TX, U.S.A., Mar. 2009.
- [2] N. Patwari and J. Wilson, "RF sensor networks for device-free localization: measurements, models, and algorithms," *Proc. IEEE*, vol. 98, no. 11, pp. 1961–1973, Nov. 2010.
- [3] J. Wilson and N. Patwari, "Radio tomographic imaging with wireless networks," *IEEE Trans. Mobile Computing*, vol. 9, no. 5, pp. 621–632, Jan. 2010.
- [4] S. Nannuru, Y. Li, M. Coates, and B. Yang, "Multi-target device-free tracking using radio frequency tomography," in *Proc. Int. Conf. Intelligent Sensors, Sensor Networks and Information Processing*, Adelaide, Australia, Dec. 2011.

- [5] J. Wilson and N. Patwari, "A fade level skew-Laplace signal strength model for device-free localization with wireless networks," *IEEE Trans. Mobile Computing*, vol. 11, no. 6, pp. 947–958, Jun. 2012.
- [6] N. Gordon, D. Salmond, and A. Smith, "Novel approach to nonlinear/non-Gaussian Bayesian state estimation," *Radar and Signal Proc., IEE Proc. F*, vol. 140, no. 2, pp. 107–113, Apr. 1993.
- [7] M. Bugallo, T. Lu, and P. Djuric, "Target tracking by multiple particle filtering," in *Proc. IEEE Aerospace Conf.*, Big Sky, MT, Mar. 2007.
- [8] S. K. Pang, J. Li, and S. Godsill, "Models and algorithms for detection and tracking of coordinated groups," in *Proc. IEEE Aerospace Conf.*, Big Sky, MT, Mar. 2008.
- [9] F. Thouin, S. Nannuru, and M. Coates, "Multi-target tracking for measurement models with additive contributions," in *Proc. Int. Conf. Information Fusion*, Chicago, U.S.A., July 2011.
- [10] ——. Multi-target tracking for measurement models with additive contributions (revised with errata). [Online]. Available: <http://networks.ece.mcgill.ca/node/189>
- [11] R. Mahler and A. El-Fallah, "An approximate CPHD filter for superpositional sensors," in *Sig. Proc., Sensor Fusion, and Target Recognition XXI, Proc. SPIE*, vol. 8392, Baltimore, MD, USA, Apr. 2012.
- [12] J. Wilson and N. Patwari, "See through walls: motion tracking using variance-based radio tomography networks," *IEEE Trans. Mobile Computing*, vol. 10, no. 5, pp. 612–621, May. 2011.
- [13] Y. Li, X. Chen, M. Coates, and B. Yang, "Sequential Monte Carlo radio-frequency tomographic tracking," in *Proc. Int. Conf. Acoustics, Speech and Signal Proc.*, Prague, May 2011.
- [14] X. Chen, A. Edelstein, Y. Li, M. Coates, M. Rabbat, and A. Men, "Sequential Monte Carlo for simultaneous passive device-free tracking and sensor localization using received signal strength measurements," in *Proc. Int. Conf. Inf. Proc. in Sensor Networks*, Chicago, U.S.A., April 2011.
- [15] D. Zhang, J. Ma, Q. Chen, and L. Ni, "An RF-based system for tracking transceiver-free objects," in *Proc. IEEE Int. Conf. Perv. Comp. and Comm.*, White Plains, NY, U.S.A., Mar. 2007.
- [16] ——. "Dynamic clustering for tracking multiple transceiver-free objects," in *Proc. IEEE Int. Conf. Perv. Comp. Comm.*, Galveston, TX, U.S.A., Mar. 2009.
- [17] D. Zhang, Y. Liu, and L. Ni, "RASS: A real-time, accurate and scalable system for tracking transceiver-free objects," in *Proc. IEEE Int. Conf. Perv. Comp. Comm.*, Seattle, U.S.A., Mar. 2011.
- [18] A. Edelstein, "Background abstraction methods for online calibration of baseline received signal strength in radio frequency sensing networks," M. Eng. thesis, McGill University, Montreal, Canada, Dec 2011.
- [19] R. Mahler, "Multitarget Bayes filtering via first-order multitarget moments," *IEEE Trans. on Aerospace and Electronic Systems*, vol. 39, no. 4, pp. 1152–1178, Oct. 2003.
- [20] F. Septier, S. Pang, A. Carmi, and S. Godsill, "On MCMC-based particle methods for bayesian filtering: Application to multitarget tracking," in *Proc. IEEE Int. Work. Comp. Adv. Multi-Sensor Adaptive Proc.*, Aruba, Dutch Antilles, Dec. 2009.
- [21] E. Mazor, A. Averbuch, Y. Bar-Shalom, and J. Dayan, "Interacting multiple model methods in target tracking: a survey," *IEEE Trans. Aerospace and Electronic Systems*, vol. 34, no. 1, pp. 103–123, Jan 1998.
- [22] A. Doucet, N. Gordon, and V. Krishnamurthy, "Particle filters for state estimation of jump Markov linear systems," *IEEE Trans. Signal Proc.*, vol. 49, no. 3, pp. 613–624, Mar. 2001.
- [23] S. Nannuru, Y. Li, M. Coates, and B. Yang, "Effect of velocity parameter on tracking for radio-frequency tomography experiments," McGill University, Tech. Rep., Aug. 2012. [Online]. Available: <http://networks.ece.mcgill.ca/node/195>
- [24] D. Schuhmacher, B.-T. Vo, and B.-N. Vo, "A consistent metric for performance evaluation of multi-object filters," *IEEE Trans. Signal Proc.*, vol. 56, no. 8, pp. 3447–3457, Aug. 2008.
- [25] S. Nannuru, Y. Li, M. Coates, and B. Yang, "Skew-Laplace model parameters for radio-frequency tomography experiments," McGill University, Tech. Rep., Apr. 2012. [Online]. Available: <http://networks.ece.mcgill.ca/node/194>



methods and random finite set approach to filtering.



and Monte Carlo inference in the application of sensor networks.



**Santosh Nannuru** is currently pursuing his doctoral studies in electrical engineering at McGill University, Canada. He received both his B.Tech and M.Tech Degrees in electrical engineering from Indian Institute of Technology, Bombay in 2009. He worked as a design engineer at iKoa Semiconductors for a year before starting his Ph.D. He is recipient of the McGill Engineering Doctoral Award (MEDA). His research interests are in signal processing, Bayesian inference, Monte Carlo

**Yunpeng Li** received the B.A. and M.S. Eng. Degrees from Beijing University of Posts and Telecommunications, China, in 2009 and 2012, respectively. He has conducted research at the Computer Networks Lab at McGill University, Montreal, Canada, in the summers of 2010 and 2011, and interned at HP Labs China, Beijing, in 2012. He will join McGill University to pursue a Ph.D. degree in electrical engineering, from September 2012. His current research is on Bayesian

**Yan Zeng** received the B.E degree in Electronic Information Science and Technology from Beijing Forestry University, China, in 2009, and M.S. Eng. degree in Communication and Information System from Beijing University of Posts and Telecommunications, China, in 2012. She is currently working at China Telecommunications Corporation as a network engineer.



and was a research associate and lecturer at Rice University, Texas, from 1999-2001. He was an Associate Editor of IEEE Transactions on Signal Processing from 2007-2011 and is currently a Senior Area Editor of IEEE Signal Processing Letters. Coates' research interests include communication and sensor networks, statistical signal processing, machine learning, and Bayesian and Monte Carlo inference.

**Mark Coates** received the B.E. degree (first class honours) in computer systems engineering from the University of Adelaide, Australia, in 1995, and a Ph.D. degree in information engineering from the University of Cambridge, U.K., in 1999. He joined McGill University (Montreal, Canada) in 2002, where he is currently an Associate Professor in the Department of Electrical and Computer Engineering. He was awarded the Texas Instruments Postdoctoral Fellowship in 1999



research interests include digital image processing, video coding and transmission, and statistical detection and estimation.

**Bo Yang** received the B.E. degree in digital communication from Beijing University of Posts and Telecommunications, China, in 1982. He joined the faculty of Beijing University of Posts and Telecommunications in 1982, where he is currently an associate professor in the School of Information and Communication Engineering, and was an associate dean of the School of Continuing Education. He is a senior member of the China Institute of Communications. His research